Materials Transactions, Vol. 49, No. 11 (2008) pp. 2497 to 2506
Special Issue on Advances in Computational Materials Science and Engineering V

Dislocation Driven Problems in Atomistic Modelling of Materials

Duc Nguyen-Manh[1], Matous Mrovec[2] and Steven P. Fitzgerald[1]

[1]*EURATOM/UKAEA Fusion Association, Culham Science Centre, Oxfordshire, OX14 3DB, United Kingdom*
[2]*Fraunhofer Institute for Mechanics of Materials IWM, Wohlerstr. 11, 79108 Freiburg, Germany*

Understanding the mechanical properties of technologically advanced materials from quantum mechanical predictions based on electronic structure calculations remains one of the most challenging problems in modern computational materials science. In this paper, we illustrate this challenge from our current investigations on dislocation behaviour in bcc transition metals that are promising candidates for materials subject to fast neutron irradiations in future fusion power plants. Starting with the relationship between the brittleness and the negative Cauchy pressure of elastic constants in materials within the so-called Harris-Foulkes approximation to the density functional theory (DFT), we briefly discuss the importance of the generic form of interatomic potentials in order to reproduce a correct Cauchy pressure. The latter in turn plays an important role in predicting dislocation properties in fcc iridium and therefore allows us to explain experimental observation of the intrinsic brittleness of this material. We then investigate the behaviour of the (1/2)[111] screw dislocation that controls plastic deformation in bcc metals from atomistic simulation. Here we show the atomic phenomena associated with the non-planar core structure of dislocations in bcc iron from the Stoner tight-binding bond model. The crucial point comes from the accurate evaluation of forces implemented within the charge neutrality conditions in the treatment of the spin-polarized dependence in the electronic structure calculations. In agreement with DFT studies, the magnetic bond-order potentials predict a non-degenerate core structure for screw dislocations in Fe. Finally, a new analytic expression has been derived for the migration energy barrier for the one-dimensional (1D) motion of crowdions, which are the most stable self-interstitial atom (SIA) defects predicted by our DFT calculations. Importantly, the latter study is strongly supported by the recent observation of 1D diffusion of nanometer-sized dislocation loops, observed very recently under in situ electron microscope irradiation for bcc transition metals.
[doi:10.2320/matertrans.MB200827]

(Received May 21, 2008; Accepted June 16, 2008; Published August 6, 2008)

Keywords: *brittle materials, Cauchy pressure, interatomic potentials, screw dislocation, crowdions, Peierls potentials, density functional theory (DFT) calculations, double sine-Gordon equation*

1. Introduction

While a broad variety of dislocation phenomena encountered in plastically deforming materials can be analysed within framework of continuum elasticity, ample evidence now exists for an important range of crystalline materials where the dislocation core structures significantly influence macroscopic plastic flow and may even be a governing factor. The properties of the core region and its impact on dislocation motion, and thus on plastic yielding, can only be fully understood when the atomistic structure and its variation with applied stresses are adequately accounted for. An immediate area of investigation is the study of the structure and properties of crystal defects in transition metals and intermetallic alloys based on transition metals, where the mixed character of covalent and metallic bonding represent a very challenging issue for understanding mechanical properties at the engineering scale. The essential precursor of such studies is an appropriate description of interatomic potentials, and this has been the main purpose of the development of environmentally-dependent bond-order potentials, which has been summarised in a recent review.[1)] These potentials have been employed in atomistic studies of screw dislocations in fcc-Ir and bcc transition metals, which revealed the non-planar character of their cores.[2)] In the last part of this paper we discuss the problem of calculating the potential energy of the migration barrier for crowdion defects created in irradiated bcc transition metals. Whereas our DFT studies have demonstrated that the crowdion configuration is the most stable one amongst self-interstitial atom defects,[3–5)] it is almost impossible to predict the small value of the migration energy of these defects, due to numerical accuracy within the first-principles calculations. Here the higher-order Frenkel-Kontorova model (which is conventionally used for the analytic description of 1D dislocation motion) has been used in conjunction with DFT calculations of the periodic substrate potentials. We find a new analytic expression for the migration potential energy, which helps to understand the experimental evidence of the low-temperature migration of crowdion defects in bcc transition metals.

2. Negative Cauchy Pressure and Brittleness in Materials

Multi-scale materials modelling of mechanical behaviour in which quantum mechanics play a crucial role has been outlined in.[6)] It is required to bridge the gap between the electronic and atomistic levels in the modelling hierarchy, and to derive inter-atomic potentials that are firmly based on the quantum mechanical predictions from DFT calculations. The electronic factors control the brittleness or ductility of single crystals indirectly, through the Burgers vectors and elastic constants. For example, in cubic crystals the ratio μ/K of shear to bulk elastic modulus has provided a useful criterion for ductility or brittleness.[7,8)] Here μ is the shear modulus on the slip plane

$$\mu = \frac{3C_{44}(C_{11} - C_{12})}{4C_{44} + C_{11} - C_{12}} \tag{1}$$

while

$$K = \frac{1}{3}(C_{11} + 2C_{12}) \tag{2}$$

and therefore we have

$$\frac{\mu}{K} = \frac{9}{(1+2A)}\left[\frac{C_{44}}{3(C_{12} - C_{44}) + (3 + 2A^{-1})C_{44}}\right] \tag{3}$$

where

$$A = \frac{2C_{44}}{(C_{11} - C_{12})}. \tag{4}$$

The argument underlying this criterion is that when the atoms at the tip of a sharp crack are strained in tension, their bonding may fail either by their slipping over another, in which case the crack becomes blunted and the crystal is ductile; or by pulling apart, in which case the crack spreads and the crystal is brittle. Cubic metal crystals are generally intrinsically ductile when $\mu/K < 0.4$ and brittle when $\mu/K > 0.5$.[8] This criterion shows why the Al crystal is ductile whereas fcc-Ir is intrinsically brittle.[9] The critical elastic property which emerged from this analysis is the Cauchy pressure term, $C_{12} - C_{44}$ (see eq. (3)) which is positive in ductile crystals but negative in brittle materials, in particular in intermetallic compounds based on transition metals. For example, the experimental value of Cauchy pressure for fcc-Ir is -13 GPa, giving $\mu/K = 0.54$, and indeed iridium is a material that undergoes both transgranular and intergranular fracture even at elevated temperature.[9,10]

The Cauchy relation between elastic constants is strongly linked to the functional form of interatomic potentials. Given the fact that pair-wise potentials produce a zero value of Cauchy pressure and that it is positive within many-body Finnis-Sinclair potentials, it was believed that the negative Cauchy pressure could be reproduced within the quantum mechanical based bond-order potentials. The latter can be obtained from the two-centre orthogonal tight-binding bond (TBB) model, in which the binding energy is written as:[11]

$$E_{\mathrm{b}} = E_{\mathrm{rep}}^{pair} + E_{\mathrm{atr}}^{bond} \tag{5}$$

where E_{rep}^{pair} is a repulsive pair-wise contribution between atoms and E_{atr}^{bond} is the covalent-bonded attractive energy. The bond energy contribution is given by

$$E_{\mathrm{atr}}^{bond} = \frac{1}{2}\sum_{I,J\neq I} E_{IJ}^{bond} = \sum_{I,J\neq I}\sum_{\alpha,\beta} H_{I\alpha,J\beta}\Theta_{J\beta,I\alpha} \tag{6}$$

in terms of the TB Hamiltonian and the bond-order matrix elements with respect to the valence orbitals α and β at atomic sites I and J, respectively. In the case of transition metals, these matrix elements are mainly determined by d-orbital contributions. The bond-order matrix elements are expressed in terms of an integral over the corresponding inter-site Green function as

$$\Theta_{I\alpha,J\beta} = -\frac{2}{\pi}\int_{-\infty}^{\varepsilon_F} \lim_{\eta\to 0} \mathrm{Im}\, G_{I\alpha J\beta}(\varepsilon + i\eta)d\varepsilon \tag{7}$$

where ε_F denotes the Fermi energy. Following eq. (5) the Cauchy relation within TBB based bond-order potentials for a cubic lattice is:

$$C_{12} - C_{44} = C_{12}^{bond} - C_{44}^{bond} + \frac{1}{2}\sigma_{11}^{bond} \tag{8}$$

Here σ_{11}^{bond} is the stress component from the bond-energy contribution (eq. (6)). The relation (8) is defined from equilibrium conditions, arising from the requirement that the system is in a minimum-energy configuration with respect to any homogeneous applied strains:

$$\sigma_{\mu\nu} = \frac{1}{\Omega}\sum_{I,K\neq I}\frac{\partial E}{\partial R_{IK}^{\mu}} R_{IK}^{\nu} = \sigma_{\mu\nu}^{pair} + \sigma_{\mu\nu}^{bond} = 0. \tag{9}$$

Applying eqs. (8) and (9) and using the OXON code[12] to calculate the bond-order potentials, we found unfortunately that the Cauchy pressure for fcc-Ir remains strongly positive, in contradiction with experimental data. In order to gain insight into the origin of the negative Cauchy pressure, we have employed density functional theory (DFT) within the Harris-Foulkes approximation (HFA)[13] from which the TBB model has been derived. A detailed examination of the different energy contributions to the elastic constants allows the conclusion that the band energy and electrostatic terms contribute to the Cauchy pressure very large cancelling positive and negative components, respectively. It is important to note that even for materials with positive Cauchy pressure (such as bcc tungsten), the electrostatic contribution is equally large and negative, and it could not be properly reproduced within eq. (5). The origin of the discrepancy between the HFA and TBB models comes from the fact that in the latter we have neglected the overlap repulsive contribution due to the high density of sp-valence electrons in the region under the strong influence of unsaturated covalent d bonds. By adding the environmental dependence to the repulsive interaction approximated by a screened Yukawa form

$$\Phi(\lambda_{IJ}R_{IJ}) = \frac{A}{R_{IJ}}\exp[-\lambda_{IJ}(R_{IJ} - 2R_{\mathrm{c}})] \tag{10}$$

where R_{c} is the core radius, and a many-body functional implemented into the screening parameter λ_{IJ}:

$$\begin{aligned} \lambda_{IJ} &= \frac{1}{2}(\lambda_I + \lambda_J) \\ \lambda_I &= \lambda_I^{atom} + \delta\lambda_I \\ \delta\lambda_I &= f(\rho_I) = \left[\sum_{K\neq I}\rho(R_{IK})\right]^{1/\gamma} \end{aligned} \tag{11}$$

to eq. (5), the environmentally dependent bond-order potentials for fcc-Ir reproduce the negative Cauchy pressure in excellent agreement with experimental data. Importantly, the constructed potential also accurately reproduces experimental phonon spectra including the anomaly in the $[\varsigma\varsigma^0]$ branch around $\varsigma = 0.5$. The intrinsic stacking faults, the extrinsic stacking fault and the twin boundary energies were found to be 408, 462 and 222 mJ m^{-2}, respectively. The agreement of the present calculated intrinsic stacking fault energy is in a very good agreement with experimental value of 420 mJ m^{-2} and it is within the range of various DFT calculations (365–445 mJ m^{-2}).[14]

We have therefore showed that the environmentally dependent bond-order potentials describing correctly not only bonding character but also elastic Cauchy relation in fcc-Ir, have predicted very well planar defect behavior. The latter is crucial for investigating mechanical properties in metals and in particular the origin of brittleness in iridium. Atomistic simulations of the $\frac{a}{2}[1\bar{1}0]$ screw dislocation employed a cylindrical block of atoms one Burgers vector thick and of radius 60 A^0 (2171 atoms). The axis of the cylinder is parallel to the $[1\bar{1}0]$ axis and periodic boundary

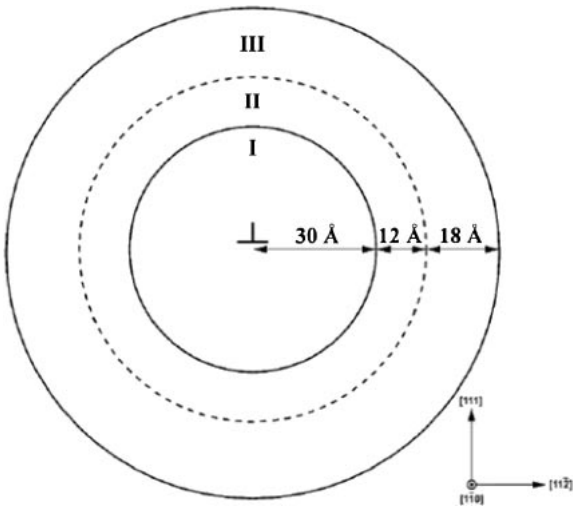

Fig. 1 Geometry of the block of atoms used in the atomistic simulation of the screw dislocation in fcc-Ir.

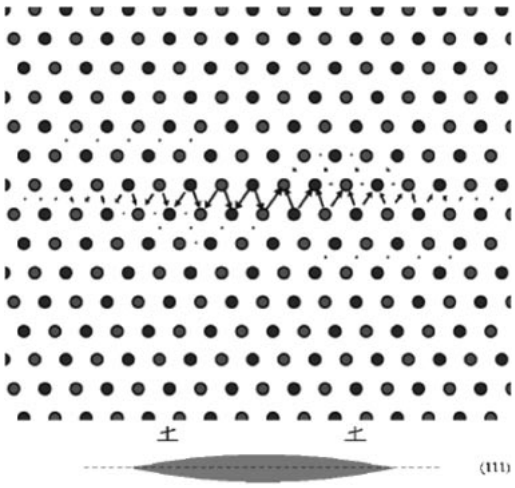

Fig. 2 Differential displacement map of the screw component of the screw dislocation in fcc-Ir using environmentally dependent TBB based bond-order potentials. The circle depict atoms in the projection onto the plane perpendicular to the dislocation line and filled coloured circles distinguish two different planes of atom within one period $\frac{a}{2}[1\bar{1}0]$.

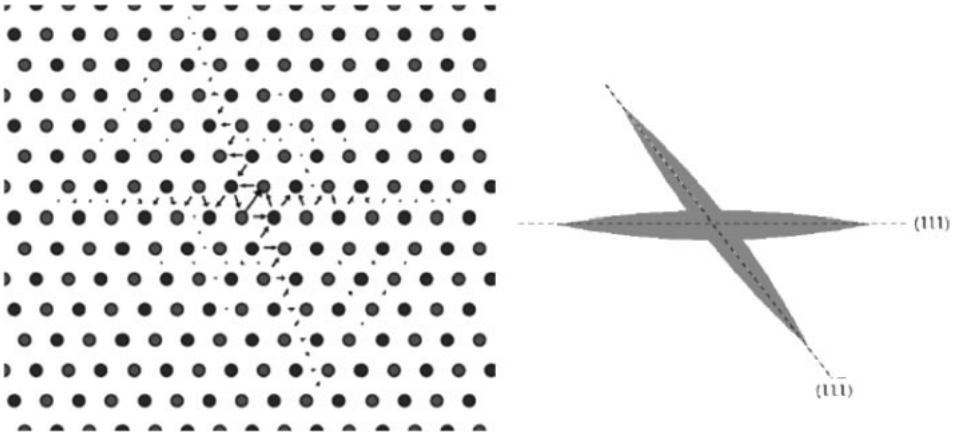

Fig. 3 The same as in Fig. 2 but for the metastable non-planar core configuration.

conditions were applied in this direction. The block was divided into three regions shown in Fig. 1. Atoms in the region I with radius $30\,A^0$ (1051 atoms) were relaxed using the molecular-static method with forces calculated from the constructed interatomic potentials. The relaxation was performed until the force acting on each atom was smaller than $0.01\,eV/A^0$, while atoms in the region II and III were held at their initial positions with the displacement field evaluated using the anisotropic elastic theory of dislocations from lattice Green function (LGF) and elastic Green function (EGF). The coordinates of all atoms in all three regions were self-consistently updated using flexible Green function boundary conditions (GFBC)[15] once the inner region was fully relaxed using the incompatibility of forces generated in the region II. The width of the region II and III is determined from the convergence of LGF and EGF solutions in fcc-Ir after atomistic relaxation which is in turn defined by a cut-off radius around given atom. We assessed several block sizes and found that the geometry given in Fig. 1 is sufficient large that further increases in the radius of region I yield identical results.

The relative displacement parallel to the total Burger vector of the neighboring atoms produced by dislocation is depicted by an arrow between them. The length of arrow is proportional to the magnitude of this displacement and it is normalized such that the length of the largest arrow is equal to the separation of neighboring atoms in the projection.

Our simulations of the $\frac{a}{2}[1\bar{1}0]$ screw dislocation found two core configurations: a planar core spreading only on the (111) slip plane (Fig. 2) and a metastable non-planar core spreading into the intersecting planes (111) and (11$\bar{1}$) of the $[1\bar{1}0]$ zone (Fig. 3). The first configuration corresponds to the conventional dissociation into two Shockley partials separated by an intrinsic stacking fault with a predicted width of splitting of $8\,A^0$ that is in an excellent agreement with high resolution transmission electron microscopy (HRTEM) observations.[16] The second core structure of the screw dislocation has never been found in atomistic simulation of other fcc elemental metals using Finnis-Sinclair (FS) and/or Embedded Atom Method (EAM) potentials, although a similar non-planar core was previously found in the intermetallic compound TiAl in the ordered fcc-like $L1_0$ structure

from our environmentally dependent bond-order potentials.[17] In order to determine which of the two core configurations is the most stable, the energy of the dislocation can be written as:

$$E_{\mathrm{dis}}(R) = E_{\mathrm{core}} + \frac{kb^2}{4\pi}\ln\left(\frac{R}{R_{\mathrm{core}}}\right) \tag{12}$$

where k is an appropriate combination of elastic constants, b is the magnitude of the total Burgers vector, R is the radial distance from the elastic centre and, E_{core}, R_{core} are the energy and radius of the core respectively. Our calculations show that the dislocation with the non-planar core is metastable, since its energy is $0.33\,\mathrm{eV}\,b^{-1}$ higher than that of the dislocation dissociated into Schockley partials. Importantly, it is shown that although the non-planar core is metastable, it can be readily formed under the effect of applied stress and may serve as an intermediate configuration for cross-slip that does not require thermal activation. In this study, the applied stress in question is the shear stress acting in {111} planes perpendicular to the Burgers vector of the dislocation (Escaig stress). These stresses do not cause glide, but may change the core structure of the dislocation. We found that the energy of the dislocation with the planar core contracted by Escaig stress of 0.025 C_{44} is almost the same as that of the non-planar core configuration. Application of stress to the dislocation with the non-planar core shows that the core can transform into a glissile planar configuration under a low value of stress (0.8×10^{-5} C_{44}). Our simulation shows that in iridium, dislocation core structure transformations lead to cross slip without the need for thermal activation. This mechanism allows cross slip to occur over long segments of the screw dislocation line with great frequency, resulting in a high number density of Frank-Read sources generated by double cross slip. When the dislocation density is sufficiently high, stress concentrators cannot be relaxed by dislocation-mediated plasticity: any cracks that form will tend to propagate rather than blunt and the materials will cleave.[18] Thus, we have shown that the origin of brittle cleavage in iridium was modelled by the results of atomistic simulations using a quantum-mechanically derived, accurate and transferable description of inter-atomic bonding in this material.

3. Modelling Dislocation Behaviour in Magnetic bcc-Fe

Body-centred cubic (bcc) transition metals and their alloys, including a wide range of ferritic/matersitic steels, have recently been identified as prime candidates for future fusion power plants, because they do not react readily with neutrons under irradiation, undergo limited swelling and helium embrittlement, and can be used with a range of possible coolants. Experiment shows that screw dislocations in bcc metals are less mobile than edge dislocations below a certain temperature, and applied stress causes mobile dislocations to be eliminated, leaving screw dislocations to control the plastic behavior. To understand the dynamics of dislocations in atomistic detail at finite temperature and under stress it is necessary to perform molecular dynamics simulations in which an accurate description of inter-atomic forces between atoms is crucial. Within the TBB based bond-order potentials, the Hellmann-Feynman force on an atom K can be evaluated from eq. (6):

$$\vec{F}_K^{bond} = -\sum_{I,J\neq I}\sum_{\alpha\beta}(\nabla_K H_{I\alpha J\beta})\Theta_{J\beta I\alpha}. \tag{13}$$

The expression (13) for the forces appears deceptively simple, since once we have evaluated the bond-order then the force is given as the gradient of the TB Hamiltonian matrix elements $H_{I\alpha J\beta}$. However, the DFT investigation of tension and compression effects on bond integrals in bcc transition metals demonstrates that there is a marked discontinuity between the first and second nearest neighbours, and therefore the continuity of two-centre TB Hamiltonian approximation in terms of conventional Slater-Koster parameters beyond the first nearest neighbours can not be accepted. This phenomena is the result of the screening of the bond integrals by the local environment, and our proposed analytic solution[19] for the screening function allows to solve the problem effectively. The screened bond-order potentials have been recently constructed for non-magnetic bcc-Mo[20] and bcc-W[21] and then tested and employed to study the core structure and glide of the screw dislocation with the Burgers vector $\boldsymbol{b} = \frac{a}{2}[111]$.

Figure 4 shows the [111] cross section of the {110} γ-surfaces for bcc-Mo calculated using screened BOP, unscreened BOP and compared with DFT calculations.[22] The energy of the $\boldsymbol{b}/3$ and $\boldsymbol{b}/6$ faults ($\gamma(\boldsymbol{b}/3)$ and $\gamma(\boldsymbol{b}/6)$), respectively, is indicated in Fig. 4 for both relaxed and unrelaxed calculations within both screened and unscreened BOPs schemes. According to Duesbery and Vitek's criterion,[23] the degenerate core comprises three faults corresponding to the displacement $\boldsymbol{b}/3$ on $(\bar{1}01)$, $(1\bar{1}0)$ and $(01\bar{1})$ planes, and the non-degenerate core comprises six faults with the displacement $\boldsymbol{b}/6$ on the same plane. For bcc-Mo, the screened BOPs give

$$\frac{6\gamma(\vec{\boldsymbol{b}}/6)}{3\gamma(\vec{\boldsymbol{b}}/3)} = 0.84 < 1, \tag{14}$$

showing that the non-degenerate core is favoured over the degenerate core. The latter result agrees excellently not only

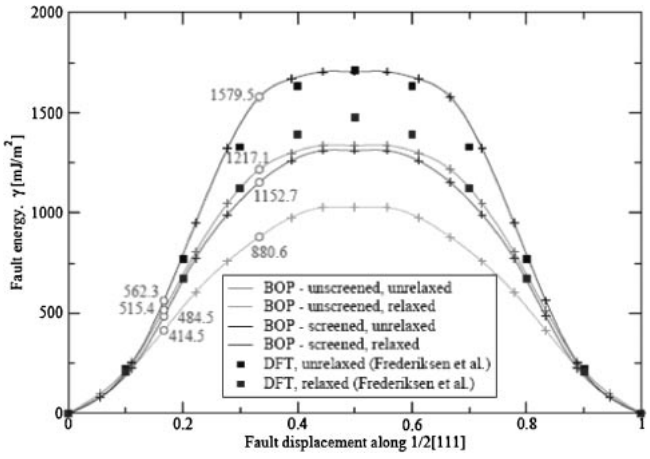

Fig. 4 The [111] cross section of the {110} γ-surfaces (in $\mathrm{mJ\,m^{-2}}$) for bcc-Mo: a comparison between unscreened BOP, screened BOP and DFT calculations.

with the atomistic simulations for the core structure of the screw dislocation in both Mo[20] and W,[21] but also with available DFT calculations[22] and explains the primary reasons for the breakdown of the Schmid law in bcc metals. More importantly we have shown that both the covalent character, originating from the angular dependence of unsaturated d-bonds, and the metallic character, coming from the screening effects of these bonds via quasi-free electrons, are equally important in an accurate description of the interatomic forces, which in turn control the dislocation behaviour in the non-magnetic bcc transition metals.

We have recently generalized the force calculation to the case of a spin-polarized TBB scheme based on the Stoner model.[1,24] In this case the Hellmann Feynman force resulting from the magnetic bond contribution can be written as:

$$\vec{F}_K^{bond} = -\sum_{\sigma=\uparrow,\downarrow}\sum_{I,J\neq I}\sum_{\alpha,\beta}(\nabla_K H^{\sigma}_{I\alpha J\beta})\Theta^{\sigma}_{J\beta I\alpha} \qquad (15)$$

where σ denotes the spin index. Within the TBB scheme, we have the on-site energies

$$H^{\sigma}_{I\alpha,I\alpha} = E_{I\alpha} \mp \frac{1}{2} I_\alpha m_{I\alpha} \qquad (16)$$

where the $E_{I\alpha}$ are adjusted to give the local charge neutrality condition in the presence of the magnetic self-consistent states; I_α denotes the Stoner parameter characterizing on-site electron exchange interaction. The magnetic moment $m_{I\alpha}$ is given by the difference between the occupation numbers of spin-up ($\uparrow$) and spin-down ($\downarrow$) states

$$m_{I\alpha} = \int_{-\infty}^{\varepsilon_{F\uparrow}} n_{I\alpha}(\varepsilon)d\varepsilon - \int_{-\infty}^{\varepsilon_{F\downarrow}} n_{I\alpha}(\varepsilon)d\varepsilon \qquad (17)$$

where $n_{I\alpha}(\varepsilon)$ is the local electronic density of states (DOS) at atom I and for orbital α. Figure 5 shows the self-consistent spin-polarized DOS for 3d states in bcc-Fe calculated within exact TB Stoner model, and magnetic bond-order potentials

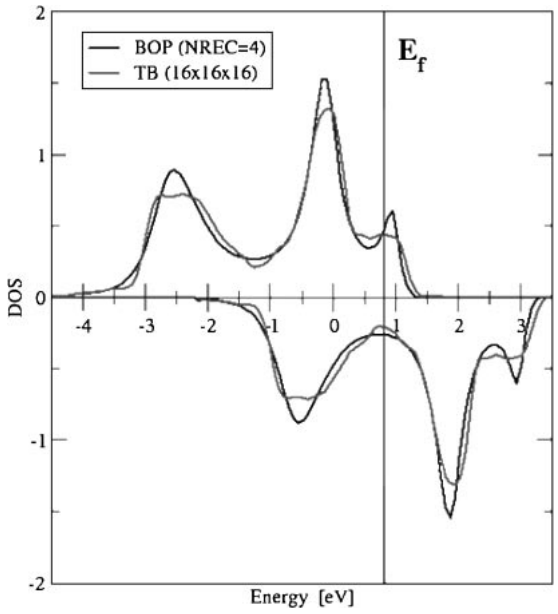

Fig. 5 Spin-polarized density of states for 3d orbitals in ferromagnetic bcc-Fe calculated within the TB Stoner scheme with $16 \times 16 \times 16$ k-points and real space BOPs.

Table 1 Elastic constants of bcc-Fe: comparison between the magnetic bond-order potentials, TB Stoner model and DFT calculations for both ferromagnetic (FM) and non-magnetic (NM) with experimental data.[25]

GPa	Exp.	DFT (FM)	TB (FM)	BOP (FM)	DFT (NM)	TB (NM)	BOP (NM)
B	172	174	168	170	314	276	324
C'	43	69	36	48	−158	−110	−149
C_{44}	116	99	118	109	141	178	101

within 4 recursion levels in evaluating the off-diagonal Green function in eq. (7).

Table 1 shows the bulk and shear moduli of both ferromagnetic and non-magnetic (NM) bcc Fe calculated by the bond-order potentials and compared with the TB Stoner model, the DFT and experimental values. Importantly, the magnetic BOPs predict that the NM bcc Fe has a negative value of $C' = \frac{1}{2}(C_{11} - C_{12})$ in agreement with other calculations, showing that the NM bcc phase is mechanically unstable. This is consistent with the high density of states at the Fermi energy found in the non-spin polarized DOS within the BOPs scheme as well as in the corresponding TB and DFT calculations for the NM bcc phase of Fe.

The core structure of the screw dislocation in magnetic iron was studied using the molecular static method, similarly as in earlier calculations for non-magnetic bcc transition metals.[20,21] The block of atoms was a parallelepiped with coordinate axes as follow: x parallel to $[\bar{1}2\bar{1}]$, y parallel to $[\bar{1}01]$ and z parallel to [111]. The dislocation with its Burgers vector $\frac{a}{2}[111]$ along the z direction was inserted in the middle of the block by applying to all atoms in the block the displacement in accordance with the anisotropic elastic field of the dislocation.[27] Periodic boundary conditions were imposed in the z direction, i.e. parallel to the dislocation line. Perpendicular to the dislocation line, in the x and y directions, the block consisted of an active region in which all the atoms are fully relaxed using magnetic BOPs, and an inactive region where the positions were held fixed but the atoms interact with those in the active region. The result of this study is shown in Fig. 6. using the usual differential displacement map. The screw component of the relative displacement of the neighbouring atoms produced by the dislocation is depicted as an arrow between them. The length of each arrow is proportional to the magnitude of these components. The core simulated by magnetic BOPs is found to be invariant with respect to the $[10\bar{1}]$ dyad, and spreads symmetrically into the three {110} planes. This core is virtually the same as that found for iron when employing DFT calculations,[26,28] but fundamentally different from that obtained by Finnis-Sinclair potentials, for which the core spreads asymmetrically.

Screw dislocations in the bcc structure can exhibit two initial configurations, termed “easy” and “hard”. These two types can be obtained from one another by reversing the Burgers vector of the dislocation while keeping the dislocation line at the same position. A comparison of these two configurations, together with a reference ideal lattice, shows that while the sequence of [111] planes in the ideal lattice is …ABC…, the sequence is changed around the dislocation centre. In the “hard” configuration, the bulk-type order of the

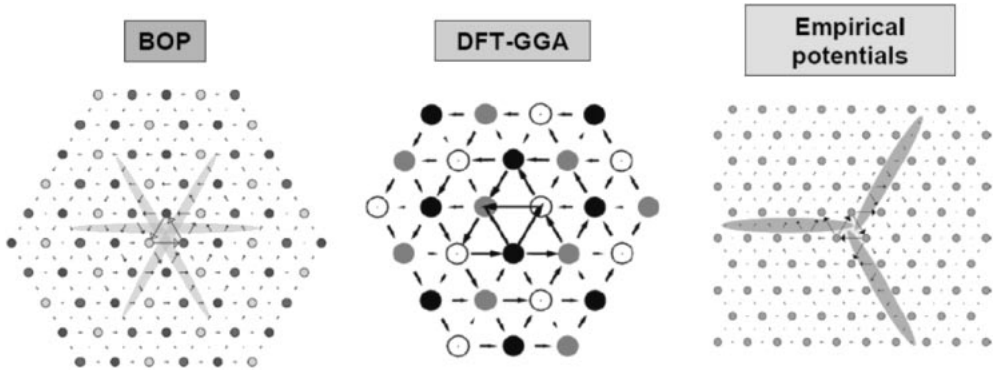

Fig. 6 Differential displacement map of the screw component for the "easy" core configuration of screw dislocation in bcc-Fe obtained from the present magnetic bond-order potentials compared with DFT-GGA calculations[26] and those from Finnis-Sinclair potentials. The atomic arrangement is shown in the projection perpendicular to the direction of the dislocation ([111]) and the circles represent atoms in the three successive (111) planes and their positions are distinguished by shadings. The arrows have the same meaning as in Figs. 2 and 3.

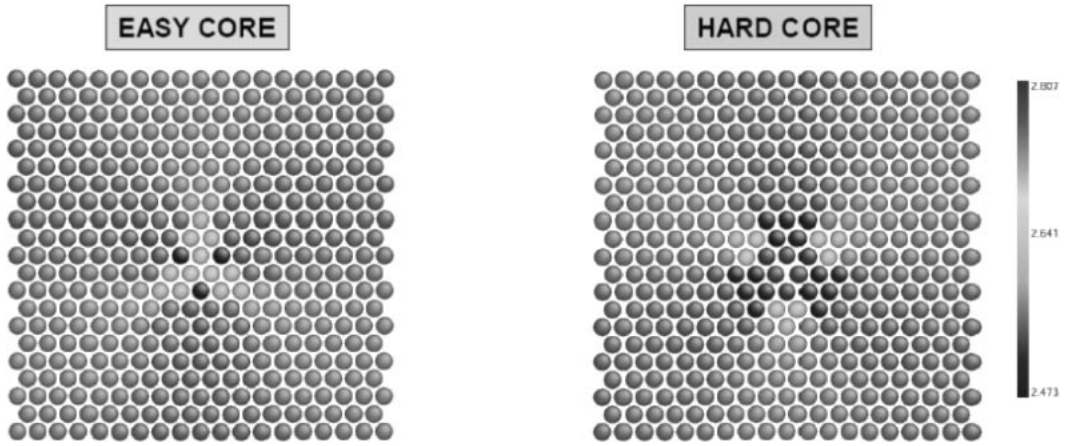

Fig. 7 Magnetic moment distributions in Bohr magneton at the core structure of screw dislocation in ferromagnetic bcc-Fe for easy and hard configurations.

neighbouring [111] atom rows that are close to the core is destroyed, and atoms from these three rows are placed in the same {111} planes. On the other hand, in the "easy" configuration, the bulk-type ordering of the three atom rows surrounding the dislocation centre is preserved but reversed in sense, so that the sequence of these rows are ...ACB....

It is found from the present magnetic BOPs study for bcc-Fe that the "easy" core configuration is energetically favourable by $0.07\,\mathrm{eV}\,\boldsymbol{b}^{-1}$ in comparison with the "hard" one, again in very good agreement with the DFT value of $0.05\,\mathrm{eV}\,\boldsymbol{b}^{-1}$.[26] Figure 7 shows the magnetic moment distribution at the two core configurations obtained from the magnetic BOPs. The magnetic moment on the three central atoms is found to be reduced by $0.2\,\mu_\mathrm{B}$ compared with the bulk value $2.62\,\mu_\mathrm{B}$ for the "easy" core, whereas it is increased by $0.2\,\mu_\mathrm{B}$ for the "hard" core configuration.

4. Analytic Potential for Crowdion Migration in Irradiated bcc Transition Metals

Unlike vacancies, self-interstitial atom (SIA) defects do not spontaneously form in metallic materials at equilibrium conditions due to their high formation energy. However, SIAs can be generated in materials employed in fusion power plants under high-energy neutron irradiation.[29] The SIA defects are remarkable because of the very large local strain field associated with their core and at the same time there are no direct experimental measurements for formation and migration energies of these defects. Our recent systematic DFT calculations for six different single SIA configurations in all bcc transition metals showed that indeed the energy of formation of single SIA defects is several times the energy of formation of a mono-vacancy.[3–5] Importantly, these studies demonstrated that in all non-magnetic bcc transition metals (V, Nb and Ta in group 5B and Mo, W in group 6B of the periodic table of elements) the ⟨111⟩ SIA configuration, or crowdion, has the lowest formation energy. For bcc-Cr where the DFT ground state is anti-ferromagnetic, the difference between the energies of the two dumbbell (⟨111⟩ and ⟨110⟩) configurations is very small. Although in ferromagnetic bcc-Fe the ⟨110⟩ SIA configuration has the lowest energy of formation, highly-mobile clusters of SIA defects observed in iron under irradiation do adopt the crowdion configuration. These SIA clusters (which are effectively prismatic dislocation loops) can migrate to sinks, and this gives rise to swelling, irradiation creep and radiation embrittlement in materials. Importantly, the systematic trend exhibited by crowdions in group 5B and 6B transition metals correlates very well with the experimental data on thermally activated migration of SIA defects, from the analysis of the resistivity

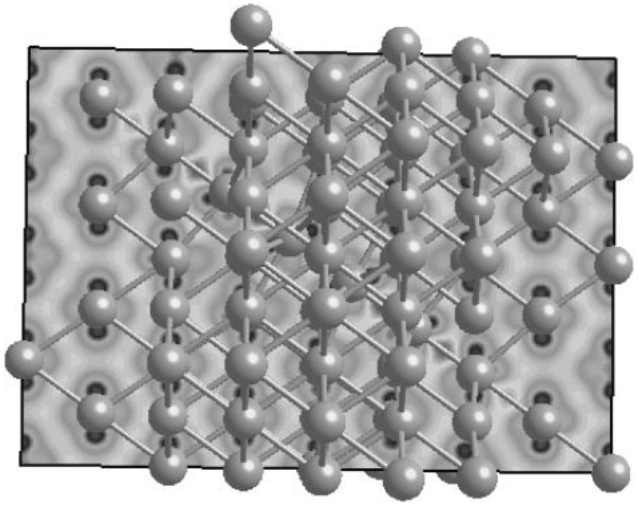

Fig. 8 Electronic charge density difference between the crowdion and the ideal bcc configurations projected on the (110) plane for tungsten from DFT calculations. The crowdion is highlighted by bond charges between atoms along the ⟨111⟩ string.

recovery curves in these materials irradiated by electrons. In the case of group 5B, the resitivity recovery measurements show that the single SIAs are already mobile at very low temperature (less than 6 K) whereas for bcc transition metals of group 6B, thermally activated migration of SIAs starts at 35 K for Mo and 27 K for W.[30)]

Figure 8 shows the relaxed atomic configuration of the crowdion obtained from a supercell calculation in bcc-W using the package of linear combination of atomic-type orbitals (PLATO) code.[31)] The self-consistent charge density associated with this configuration is projected in the (110) plane and in order to visualise the defect configuration it is subtracted from the charge density of atoms in the ideal bcc lattice. It is interesting to note that this SIA point defect transforms effectively into a peculiar line defect configuration along the [111] direction, due to the high strain field associated with the core structure of the crowdion.

Our DFT study shows that the energy difference between the ⟨110⟩ and ⟨111⟩ SIA configurations has a group-specific character: it is systematically smaller in group 6B than in group 5B of bcc transition metals. The group-specific dependence of defect properties can be with their electronic structure, especially with the ratio of number of valence electrons per atom. Figure 9 shows the local DOS for atoms forming the central string in the crowdion configuration, calculated for two representative bcc transition metals in group 5B (vanadium) and 6B (tungsten). Starting with the atom in the core of the crowdion (denoted as atom 1) to the atom situated at the end of the ⟨111⟩ string (atom 5), we see clearly the change of the local DOS behaviour from the defect to the bulk bcc lattice shape, in particular at the Fermi energy position ($\varepsilon_F = 0$). A striking feature seen in Fig. 9, is the upward shift of the anti-bonding states in comparison with the bulk spectrum of DOS. Because of the strong compressive strain in the core, the pseudogap in the bcc DOS near the Fermi energy practically vanishes for atoms 1, 2 and 3, and that is the main reason why simple many-body potentials based on the second moment approximation to the DOS can be used to model the crowdion behaviour.[5)] For an atom located sufficient far from the core (atom 5), the anti-bonding peak is shifted back to the bulk position. The magnitude of this shift is increased from group 5B (1.1 eV for vanadium) to group 6B (1.7 eV for tungsten) and its scale is sufficiently large to be observed in electron energy loss spectroscopy (EELS) measurements.

Atomic displacement fields of the central string in the crowdion found in our DFT calculations are shown in Fig. 10 for bcc-W in the $4 \times 4 \times 4$ supercell, and compared with those with a larger supercell ($9 \times 9 \times 9$) using empirical interatomic potentials. It appears to be possible to formulate a simple yet still fairly accurate analytical solvable model (the so-called Frenkel Kontorova model[32)]) describing not only individual ⟨111⟩ crowdion defect but also clusters of crowdions via the Lagrangian:[5,33,34)]

$$L = \sum_j \left\{ \sum_{n=-\infty}^{\infty} \left[\frac{m}{2} \left(\frac{\partial z_{j,n}}{\partial t} \right)^2 - \frac{\beta}{2} (z_{j,n+1} - z_{j,n} - a)^2 \right] - \sum_h \sum_{n=-\infty}^{\infty} V(z_{j,n} - z_{j+h,n}) \right\}. \tag{18}$$

Here, $z_{j,n}(t)$ denotes the position of an atom n in the direction of string j, m is the atom mass, β is the parameter of elastic

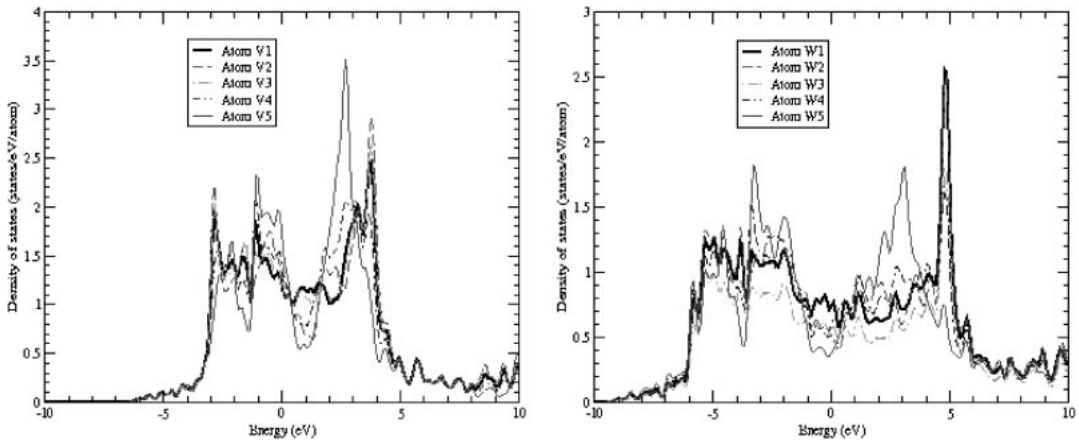

Fig. 9 Local electronic DOS calculated for 5 non-equivalent atoms along the ⟨111⟩ string of crowdion in a super-cell $4 \times 4 \times 4$ of bcc-V (left) and bcc-W (right). Atom 1 represents the core of the defect.

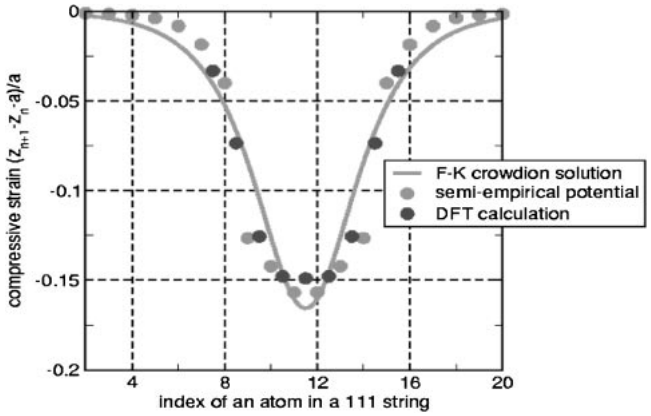

Fig. 10 Displacement fields of crowdion in bcc-W calculated by DFT technique and compared with those obtained from semi-empirical potential developed in[5] and with the analytical solution of single sine-Gordon equation.

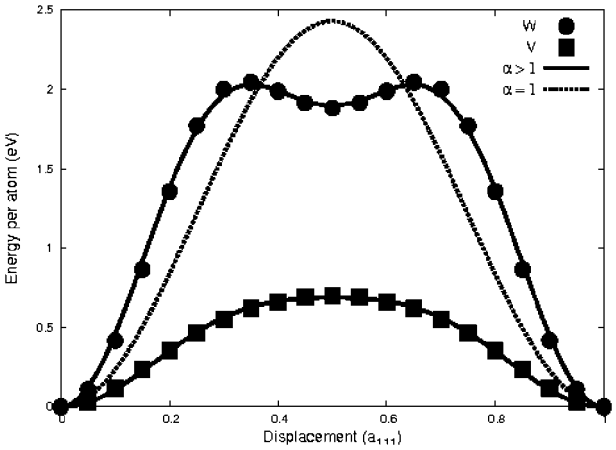

Fig. 11 Substrate potentials calculated by DFT for bcc-V (filled square) and bcc-W (filled circles) and fitted with the function $V(z)$ from eq. (22) (solid lines). For comparison, the conventional potential $V(z)$ from eq. (19) is also plotted for bcc-W (dashed line).

interaction between atoms belonging to the same string, and they interact with the surrounding "perfect" lattice via a periodic potential V. The latter is conventionally taken to be in the form

$$V(z) = V_0 \sin^2\left(\frac{\pi z}{a}\right) \tag{19}$$

where a is the equilibrium spacing between atoms in the closed packed string; for the bcc lattice $a = \frac{\sqrt{3}}{2} a_0$ with a_0 the lattice constant. In the continuum limit, eq. (18) with the periodic potential (19) has the static solution for displacement field at $j = 1$ as:

$$u(z) = \frac{2\pi}{a} \arctan\{\exp[-\mu(z - z_0)]\} \tag{20}$$

that is well-known as the solution of the single sine-Gordon equation. Here the relative strength between the interaction with the lattice (V_0) and the interaction within the string (β) is characterized by the parameter μ, defined as:

$$\mu^2 = \frac{2\pi^2 V_0}{\beta a^4}. \tag{21}$$

The solid line in Fig. 10 shows the analytic solution (eq. (20)) which away from the central core region agrees qualitatively with the results of DFT calculations. The outstanding problem with the crowdion defect is that an accurate evaluation of its migration energy would be extremely difficult within a supercell DFT calculation.[3–5] Although the DFT numerical error of 0.01 eV is acceptable for evaluating the migration energy of mono-vacancies in bcc transition metals (ranging from 0.62 eV in vanadium to 1.78 eV in tungsten) within the nudged elastic band technique,[3,4] it appears to be unacceptable for predicting the migration energy of the crowdion, which is already mobile at very low temperature as observed in the resistivity recovery experiments.

In order to have a more quantitative evaluation of the migration energy for the crowdion, we have performed a systematic study of the periodic substrate potential interaction, $V(z)$, in eq. (18). These were determined by considering a defect-free lattice and calculating the energy per atom of one of the ⟨111⟩ strings as it was rigidly displaced relative to its neighbours along the axis. Figure 11 shows the DFT-calculated potentials for bcc-V and bcc-W. In all bcc transition metals in group 5B, our calculations show the same structure of a flattening peak, whereas a structure with a local minimum at the middle point of the ⟨111⟩ displacement is characteristic of the metals in group 6B. The DFT results for the substrate potentials showed that the function $V(z)$ of eq. (19) is not appropriate for modelling the periodic potential in the Lagrangian (18). It can be seen clearly in the case of bcc-W that this function (dashed line in Fig. 11) cannot be used to fit the DFT data.

A more general function which can be fitted accurately to the potentials calculated via DFT is the double-sine potential:

$$V(z) = V_0\left[\sin^2\left(\frac{\pi z}{a}\right) + \frac{\alpha^2 - 1}{4}\sin^2\left(\frac{2\pi z}{a}\right)\right] \tag{22}$$

with an additional parameter α. This function is more flexible and in the limit of $\alpha \to 1$ it returns to the form of eq. (19). As α increases above 1 the peak flattens as in the case of bcc-V ($\alpha = 1.31$) and when $\alpha > \sqrt{2}$, $V(z)$ contains a minimum at $z = (a/2)$ as in the case of bcc-W ($\alpha = 1.64$). Figure 11 shows that the solid lines representing the function (22) fit excellently with DFT data for both vanadium and tungsten. Within the continuum limit, the Lagrangian (18) with the potential (22) has the double-kink like solution for a single crowdion

$$u(z) = \frac{a}{\pi} \arctan\left\{\frac{\alpha}{\sinh[\mu\alpha(z - z_0)]}\right\} \tag{23}$$

which was first derived in Ref. 35) in the context of a kinked dislocation line. The total potential energy associated with the crowdion can be written as

$$E = \int_{-\infty}^{\infty} \left\{\frac{\beta a^2}{2}\left(\frac{\partial u}{\partial z}\right)^2 + V[u(z)]\right\}. \tag{24}$$

Since $u = u(z - z_0)$ this integral is independent of z_0

$$E_0 = \frac{a}{\pi}\sqrt{2V_0\beta}\left(\alpha + \frac{\cosh^{-1}\alpha}{\sqrt{\alpha^2 - 1}}\right) \tag{25}$$

where E_0 denotes the total potential energy in the continuum approximation. Physically, this corresponds to the period of lattice potential going to zero, and in this approximation the crowdion can move freely through the crystal. In order to evaluate the migration potential (Peierls potential) for the crowdion, we have to take into account the discreteness of the lattice, and the expression (25) can be viewed as the zero order approximation. The simplest way to take into account the discreteness is to use the solution (23) and calculate the static potential of an atomic chain with a crowdion by using the formula

$$E = \sum_{n=-\infty}^{\infty} \left[\frac{\beta}{2} (u_{n+1} - u_n)^2 + V(u_n) \right]. \tag{26}$$

It can be assumed that the same equal energy distribution remains in a discrete chain of atoms and instead of eq. (26) we can write

$$E = 2 \sum_{n=-\infty}^{\infty} V(u_n) = E_0 + U(z_0) \tag{27}$$

where the first term E_0 is the same as eq. (25) and the second term $U(z_0)$ represents the potential landscape the crowdion as a whole experiences, dependent on its centre of mass z_0. The analytic expression for $U(z_0)$ has been found very recently in Ref. 36) and the potential barrier heights for V and W have been calculated. The calculated migration barriers for crowdion in V and W are $6.8\,10^{-4}$ eV and $2.6\,10^{-3}$ eV and the corresponding estimated migration temperatures are 8 K and 30 K that are in very good agreement with the experimental data of 6 K and 27 K, respectively.

5. Conclusions

We have presented three problems illustrating mathematical challenges in the atomistic modelling of dislocation behaviour that is crucial for investigating the mechanical properties of materials at the engineering scale. We have shown that DFT and tight-binding analysis of the Cauchy relations between elastic constants is important to understand the generic functional form of interatomic potentials for modelling brittleness of materials such as fcc iridium. Here the prediction of a metastable non-planar core configuration of the screw dislocation allows us to propose a cross-slip mechanism for multiplication of dislocation density and strong work hardening from which brittle cleavage is a natural consequence. In the case of the screw dislocation in bcc transition metals, we demonstrated that the discontinuity of quantum-mechanically based forces found from DFT studies compression/tension effects on bonding properties between the first and second nearest neighbour's atoms is the key point to predict the core structure of the screw dislocation. We have used the tight-binding Stoner model to construct the magnetic bond-order potentials for bcc iron. This allows us to investigate the displacement field around the core structure of dislocation as a function of magnetic moments. We would like to stress here that the core structure phenomena in bcc transition metals at the atomistic level percolate though the nano- and meso-scale to the macroscopic scale, helping to understand the plastic behaviour of these materials at the engineering level. Finally in the case of irradiated bcc materials where SIA defects play an important role, we have shown that by linking DFT prediction of the crowdion as the most stable SIA configuration in non-magnetic bcc transition and also DFT calculations of the periodic substrate potentials along the $\langle 111 \rangle$ string, it is now possible to find an analytical expression for the Peierls potentials for crowdion migration. The latter have been calculated for bcc-V and bcc-W and they are in an excellent agreement with resistivity recovery measurements. More importantly, it is shown that the link between continuum and discrete mechanics is pivotal for understanding dislocation behaviour in irradiated bcc transition metals[37] where the one-dimensional diffusion of nanometer-sized dislocation loops has been observed under in situ electron microscopy measurements.

Acknowledgements

This paper is dedicated to Professor Y. Kawazoe on the occasion of his 60th birthday. The authors would like to thank M. J. Cawkwell, S. L. Dudarev, R. Groger, D. G. Pettifor and V. Vitek for stimulating discussion. DNM and SPF are supported by the UK Engineering and Physical Sciences Research Council and the European Community under the contract of Association between EURATOM and UKAEA. The views and opinions expressed herein do not necessary reflect those of the European Commission.

REFERENCES

1) D. Nguyen-Manh, V. Vitek and A. P. Horsfield: Progress in Materials Science **52** (2007) 255–298.
2) D. Nguyen-Manh, M. J. Cawkwell, R. Groger, M. Mrovec, R. Porizek, D. G. Pettifor and V. Vitek: Mater. Sci. Eng. A **400–401** (2005) 68–71.
3) D. Nguyen-Manh, A. P. Horsfield and S. L. Dudarev: Phys. Rev. B **73** (2006) 020101R.
4) D. Nguyen-Manh, S. L. Dudarev and A. P. Horsfield: J. Nucl. Mater. **367–370** (2007) 257.
5) P. M. Derlet, D. Nguyen-Manh and S. L. Dudarev: Phys. Rev. B **76** (2007) 054107.
6) D. Nguyen-Manh, A. M. Bratkovsky and D. G. Pettifor: Phil. Trans. R. Soc. Lond. A **351** (1995) 529–542.
7) S. F. Pugh: Phil. Mag. **54** (1954) 823.
8) A. H. Cottrell: Mater. Sci. Tech. **5** (1989) 1165
9) S. S. Hecker, D. L. Rohr and D. F. Stein: Metall. Trans. **9A** (1978) 481.
10) P. Panfilov, V. Novrogodov and A. Yermakov: J. Mater. Sci. Lett. **13** (1994) 137.
11) M. Aoki, D. Nguyen-Manh, D. G. Pettifor and V. Vitek: Progress in Materials Science **52** (2007) 154–195.
12) OXON code, A. P. Horsfield, D. R. Bowler, A. M. Bratkovsky, M. Fearn, P. Goodwin, S. Goedecker and D. Nguyen-Manh: Oxford University, 2001; http://www-mml.materials.ox.ac.uk/facilities/oxon.shtml
13) D. Nguyen-Manh, D. G. Pettifor, S. Znam and V. Vitek: *Tight-binding approach to computational materials science*, Eds. P. E. A. Turchi *et al.* (MRS Symposium Proceeding, **491**, 1998) 353–358.
14) M. J. Cawkwell, D. Nguyen-Manh, D. G. Pettifor and V. Vitek: Phys. Rev. **B73** (2006) 064104.
15) C. Woodward and S. I. Rao: Philos. Mag. **84** (2004) 401.
16) T. J. Balk and K. J. Hemker: Philos. Mag. **A81** (2001) 1507.
17) S. Znam, D. Nguyen-Manh, D. G. Pettifor and V. Vitek: Philos. Mag. **83** (2003) 415.
18) M. J. Cawkwell, D. Nguyen-Manh, C. Woodward, D. G. Pettifor and V. Vitek: Science **309** (2005) 1059–1062.
19) D. Nguyen-Manh, D. G. Pettifor and V. Vitek: Phys. Rev. Lett. **85**

(2000) 4136–4139.
20) M. Mrovec, D. Nguyen-Manh, D. G. Pettifor and V. Vitek: Phys. Rev. B **69** (2004) 094115.
21) M. Mrovec, R. Groger, A. G. Bailey, D. Nguyen-Manh, C. Elsasser and V. Vitek: Phys. Rev. B **75** (2007) 104119.
22) C. Woodward and S. I. Rao: Phys Rev. Lett. **88** (2002) 6402.
23) M. S. Duesbery and V. Vitek: Acta Mater. **46** (1998) 1481.
24) S. Chatasiriwan and F. Milstein: Phys. Rev. B **58** (1998) 5996.
25) G. Q. Liu, D. Nguyen-Manh, B. G. Liu and D. G. Pettifor: Phys. Rev. B **71** (2005) 174415.
26) L. Ventelon and F. Willaime: J. Computer-Aided Mater. Des. **14** (2007) Supplement 1, 85.
27) J. P. Hirth and J. Lothe: *Dislocation Theory*, (New York, Wiley, 1982).
28) S. L. Frederiksen and K. W. Jacobsen: Philos. Mag. Lett. **83** (2003) 365.
29) I. Cook: Nature Materials **5** (2007) 77.
30) P. Ehrhart, P. Jung, H. Shultz and H. Ullmaier: Atomic Defects in Metals, Eds. H. Ullmaier, Landolt-Bornstein, New Seriers, Group III, **25**, (Spinger-Verlag, Berlin, 1991).
31) S. D. Kenny, A. P. Horsfield and H. Fujitani: Phys. Rev. B **62** (2000) 4899.
32) O. M. Brawn and Y. S. Kivshar: *The Frenkel-Kontorova model*, (Spinger, 2004).
33) A. M. Kosevich: *The Crystal Lattice*, (Wiley-VCH, 1999).
34) S. L. Dudarev: Philos. Mag. **83** (2003) 3577.
35) F. C. Frank and J. H. van der Merwe: Proc. Roy. Soc. Lon. **A200** (1949) 125.
36) S. Fitzgerald and D. Nguyen-Manh: *In Electron Microscopy and Multiscale Modelling, EMMM-2007 Proceeding Conference*, Eds. A. S. Avilov, S. L. Dudarev and L. D. Marks, (2008, AIP), 93–101.
37) K. Arakawa, K. Ohno, M. Isshiki, K. Mimura, M. Ichikoshi and H. Mori: Science **318** (2007) 956.